Failure Analysis of a Welded Steel Pipe at Kullar Fault Crossing.

FAILURE ANALYSIS OF A WELDED STEEL PIPE AT KULLAR FAULT CROSSING

Ercan Serif Kaya[1], Eren Uckan[2*], Michael J.O'Rourke[3], Spyros A. Karamanos[4], Bulent Akbas[5], Ferit Cakir[6], Yin Cheng[2]

[1]Dept. of Civil Engineering, Alanya Alaaddin Keykubat University, Antalya, Turkey

[2*]Corresponding author, Dept. of Earthquake Engineering, Kandilli Observatory and Earthquake Research Institute (KOERI), Bogazici University, Istanbul, Turkey

[3] Dept. of Civil and Environmental Engineering, Rensselaer Polytechnic Institute, NY, USA

[4] Dept. of Mechanical Engineering, University of Thessaly, Volos, Greece

[5]Dept. of Civil Engineering, Gebze Technical University, Kocaeli, Turkey

[6] Dept. of Architecture, Yildiz Technical University, Istanbul, Turkey

Abstract

The seismic response of a 2200-mm-diameter welded steel pipe at strike slip Kullar fault crossing in Izmit, Kocaeli during 1999 Kocaeli earthquake is investigated. The pipe was crossing the fault-line with an angle of 55 degrees and suffered leaks due to 3.0 m of right lateral movement of fault, which imposed compressive axial strain in the pipe. The backfill material of the trench was native soil which was non-homogenous (soft and stiff clay) with respect to fault line-soft material on the North side, stiff material on the South side. Field observations revealed two major wrinkles with finger width cracks and a minor wrinkle on the soft soil side of the fault. Large plastic strains and local folding were observed at wrinkles due to compressive strains. The case is known as one of the best documented fault crossing examples.

The failure behavior of the Thames Water pipe during 1999 Kocaeli earthquake is simulated by utilizing a 3D nonlinear continuum FE model. The numerical model considers contact surface at soil pipe interface and performs large deformation analyses of the pipe. The locations of wrinkles as well as axial displacements/rotations demands due to fault rupture are predicted. It is observed that once wrinkle initiates, strain in the pipe away from the wrinkle reduces after initial local buckling and additional shortening of the pipeline tends to accumulate at the wrinkle causing large plastic strains and rotation demands associated with fault rupture, an observation consistent with field observations and 2005 ALA guidelines.

Keywords: Buried steel pipes; pipe failure; local buckling; fault crossing; Kocaeli earthquake

1. Introduction

Welded steel pipelines are commonly used in transmitting oil, gas and water from the sources to end users. Such high quality pipes usually do not suffer damage due to wave propagation but can be damaged by permanent ground deformations (PGD) caused by surface faulting, landslides and liquefaction induced lateral spreads. Among these, the fault crossing hazard is considered as one of the most severe as such abrupt ground deformations (step loadings) may cause excessive axial strains in the pipe wall and lead to failure.

The main aim in the design of buried pipelines in fault crossing areas is to reduce the risk of damage due to fault displacements by minimizing the pipe strains. Axial and lateral nonlinear soil springs are used to represent the soil resistance to pipe movement in numerical modeling. The design strategy is to promote tension as opposed to compression in the pipe and to adjust the orientation angle, slip direction, pipe thickness and soil backfill material of the soil so as to minimize axial strains in the pipe[1-4]. The compression failure of the pipeline takes place at lower offset values than failure in tension [5] and therefore it should be avoided in the design of pipes. However, pipe orientation and crossing angles are often governed by right-of-way constraints which are also included in the current design codes. Nevertheless, in the past, relevant provisions or guidelines were not available in pipeline design practice. A simplified model has also been developed by Uckan*et al.* which is commonly needed for engineering practices to determine the seismic demand of steel pipes at fault crossings [6].

The behavior of steel pipes under compression is quite complex, associated with a series of events that may lead to pipeline failure. Therefore, case studies on pipe wall failure are particularly important to understand the actual behavior of pipes subjected to fault displacements. The behavior of a pipe segment subjected to compressive loading has been the subject of several publications in the past. Notable contribution on the buckling failure of steel tubular members and pipes subjected to pure axial compression have been reported by Reid [7], and more recently by Tutuncu [8] and Bardi and Kyriakides [9]. The bending response and buckling of tubulars have been reported by Ju and Kyriakides [10], Karamanos and Tassoulas [11] and recently in a study by Sarvanis *et al*. [12] of the behavior of large-diameter spiral-welded pipes. Furthermore, the effect of surrounding soil restrain on the buckling strength of buried pipelines has been studied by Youn and Kyriakides [13].

In the 1999 Kocaeli earthquake, the main 2200-mm-diameter butt-welded steel Thames Water Transmission Pipeline experienced major damage and leaks due to rupture of the strike slip fault, a branch of the Sapanca segment of the North Anatolian Fault (NAF). The pipe was constructed one year before the 1999 Kocaeli earthquake. It was crossing the fault with an angle of 55 degrees and subjected to net compression due to 3 m of right lateral slip. It was a severe situation for the pipeline. As a result, the pipe suffered two major and one minor local buckles, shortened by 1.7 m, underwent large axial plastic strains. However, it stayed in service after the earthquake before the repairs were made[14].

A number of researchers investigated the performance of the Thames water pipe [14-18]. Liu *et al*. used a shell model for equivalent boundary [18].Takada used simplified methods to estimate the maximum strain considering material and geometric nonlinearities [19]. Liu *et al.* investigated the relation between the maximum strain and bending angle was studied by using beam shell hybrid finite element model [20]. They used equivalent soil springs, adopted from ASCE 1984 [21], to consider the effects of soil resistance to pipe movement. The effects of internal pressure were taken into account indirectly by increasing the pipe wall thickness from 18 mm to 28 mm [18]. A series of nonlinear analyses are performed to estimate the response of the pipeline. The location of the wrinkles and the average strain at these locations were captured. A detailed field survey and a numerical analysis were conducted by Eidinger and O'Rourke, Parker, Tang and Liu [14-18]. It was observed that though localized strains exceeded 20% in many locations, the rupture of the pressure boundary (tearing of the pipe wall) happened only at a single location and a small surface leak was observed where the pipe crosses the fault. The distance between the two large wrinkles was found to be 17 m. The axial shortening and lateral offsets were calculated as 1.7 m and 2.47 m, respectively by assuming that the fault moves in a pure strike slip fashion [9]. The area map and schematic representation of the fault and pipeline are provided by Eidinger [15] in Fig. 1-2.

This paper aims to investigate the response of Thames water transmission pipeline by utilizing a three dimensional (3D) nonlinear continuum model. This type of modeling has been also introduced in [22], and offers a powerful tool for buried pipeline analysis. The effects of large deformations of the pipe, contact boundary at the pipe-soil interface, pipe internal pressure and pipe-end boundary conditions are considered.

In previous researches, the beneficial effect of pipe internal pressure on pipe response was considered explicitly by increasing the thickness of the pipe wall [18]. Moreover, the effects of boundary conditions on the structural response were also ignored. In this research we have analyzed the pipe-soil interaction model by utilizing a full 3D nonlinear continuum FE model in which the effects of internal pressure is considered. The axial resistance of the soil is represented by equivalent boundary springs located at the end of pipe. The properties of the boundary spring are calculated through simplified models as described in (Appendix.1). Observed and calculated hinge separation distances (Appendix.2) are compared as a crosscheck to the FE model. Initial local buckling(onset of buckling) and response of the pipe in the post elastic phase are investigated.

2. The Observed behavior of Thames Water Pipeline

Kullar fault is a branch of western segment (Sapanca) of the North Anatolian Fault (NAF), in Izmit, Kocaeli. The location of Thames water transmission pipeline at Kullar fault crossing is shown in the satellite image (Fig.1). The southern block moves towards west (left) with respect to northern block with a displacement of 3.0 m during the earthquake.

Water is delivered to Izmit from the Yuvacık Dam via a water treatment plant in Kullar where the fault was crossing the pipe with an angle of β = 55°. The fault ruptured about 3.0 m in right lateral fashion causing axial compressive strains in pipe. The lateral and axial components of the fault offset were 2.30 to 2.47 m and 1.7 m, respectively [15]. The locations of wrinkles and observed damages in the pipe are shown in Fig. 2 and 3.

Two major wrinkles were observed at both side of the fault line. First wrinkle is located on the stiff side (southern block) about 3 m to the south of fault line, whereas second wrinkle on the soft side (northern block) of fault, about 14.0 m way to the north of fault line. Third minor wrinkle occurred at a distance of about 14.0 m from the second wrinkle in the soft soil region as shown in Fig. 2.

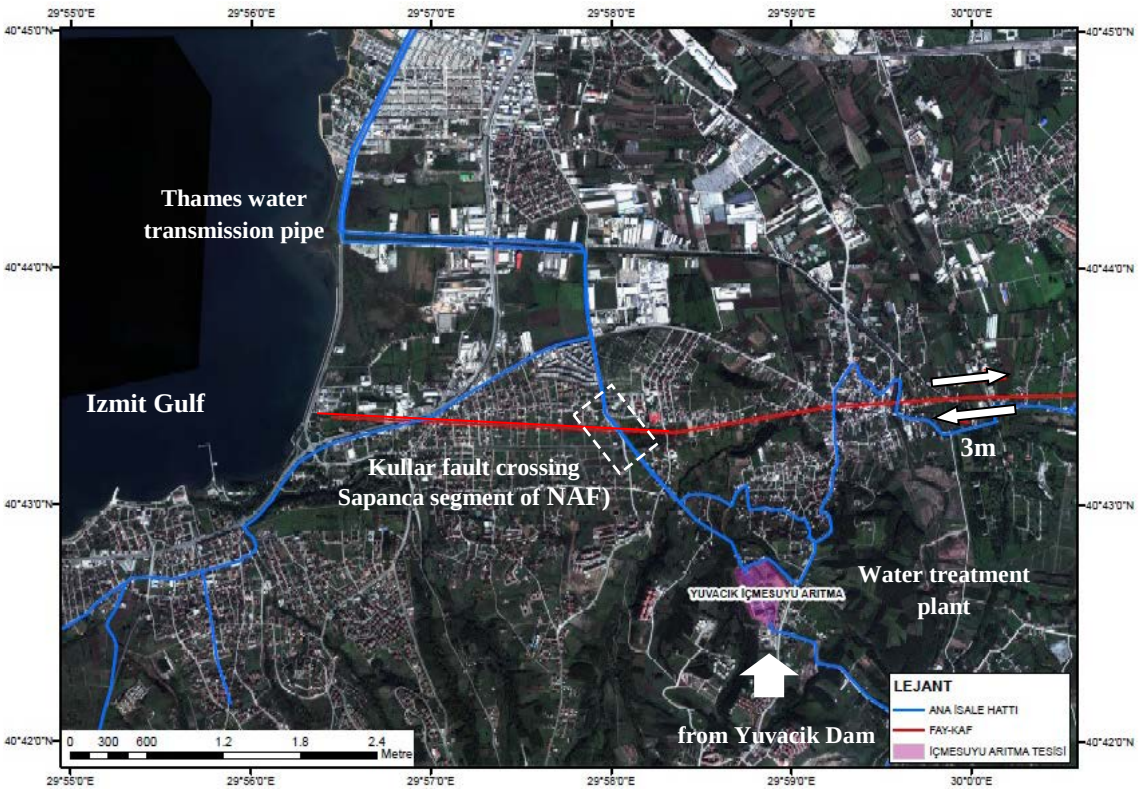

Fig. 1. *The Thames water transmission pipeline at Kullar fault crossing, (Satellite image by ISU)*

Pipe wrinkling caused a reduction in the net pipe cross section. The extend of the wrinkles suggested that the internal diameter had been necked down to about 1.4 m diameter (from 2.2 m) at two major wrinkles, (Fig. 3). Geotechnical studies revealed that native soil on both sides (Northern and Southern) of the fault line consist of soft and stiff clay, respectively.

Generally older steel pipe with gas-welded joints often rupture at relatively small strain levels due to the reduced ductility of the weld area. Heat-affected zone (HAZ) and base metals, modern corrosion-free steel pipes with arc-welded butt joints have been shown to be capable of resisting significant inelastic deformation before rupture[14, 15]. Tearing (rupture) of the Thames Water pipe wall was reported to happen along the (HAZ), close to the butt weld joint.

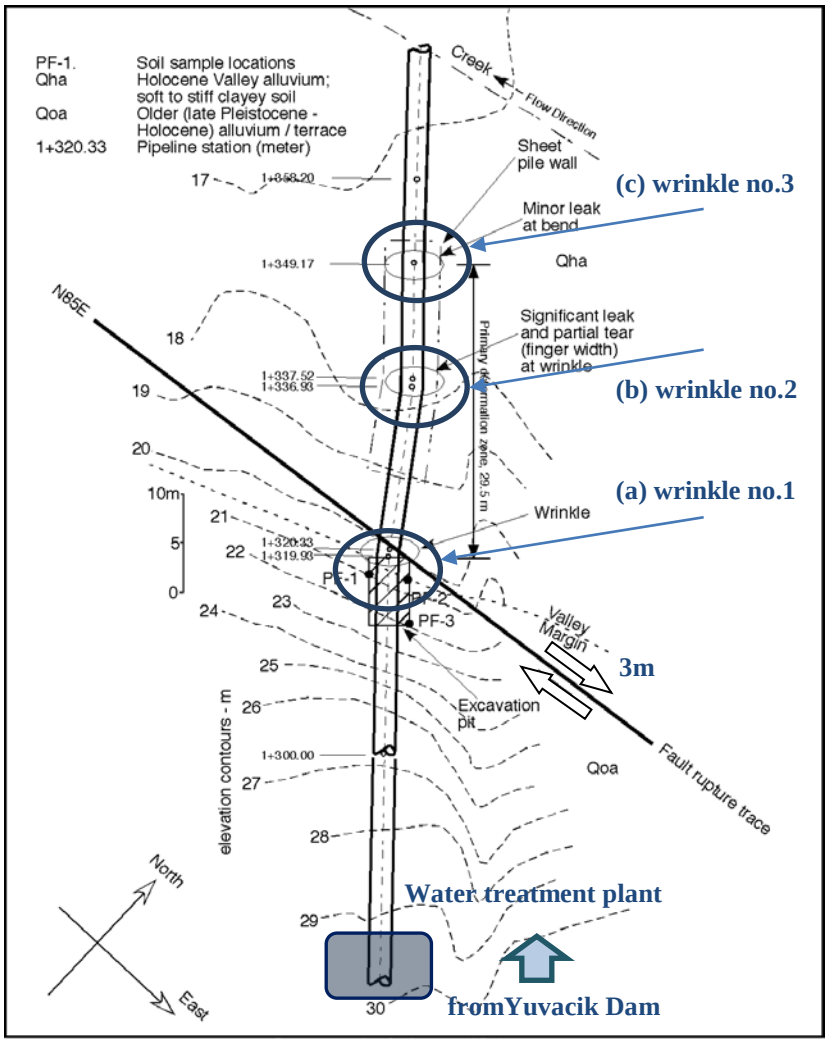

Fig. 2. *Schematic representation of the locations of two major and one minor wrinkles of Thames Water Pipeline (Eidinger* [9]*)*

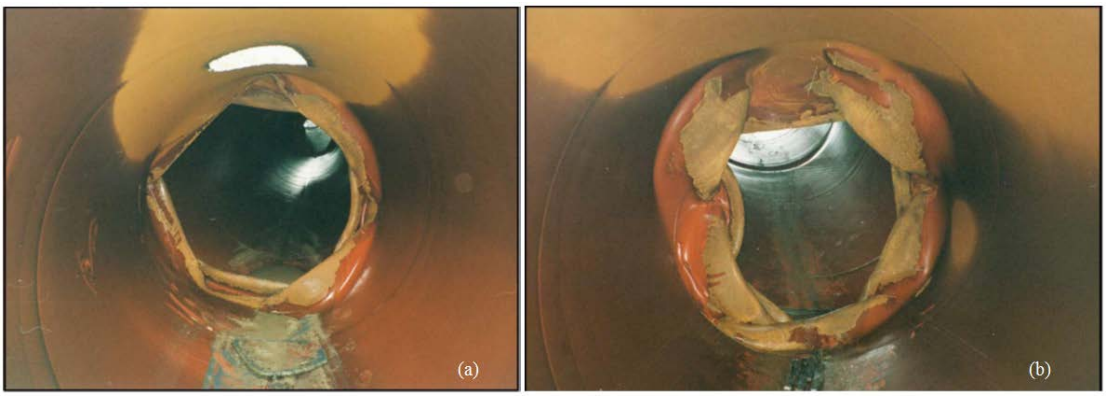

Fig. 3. *Reduction of the internal diameter due to wrinkling (a) view from North towards South (b) view from South towards North* [14]

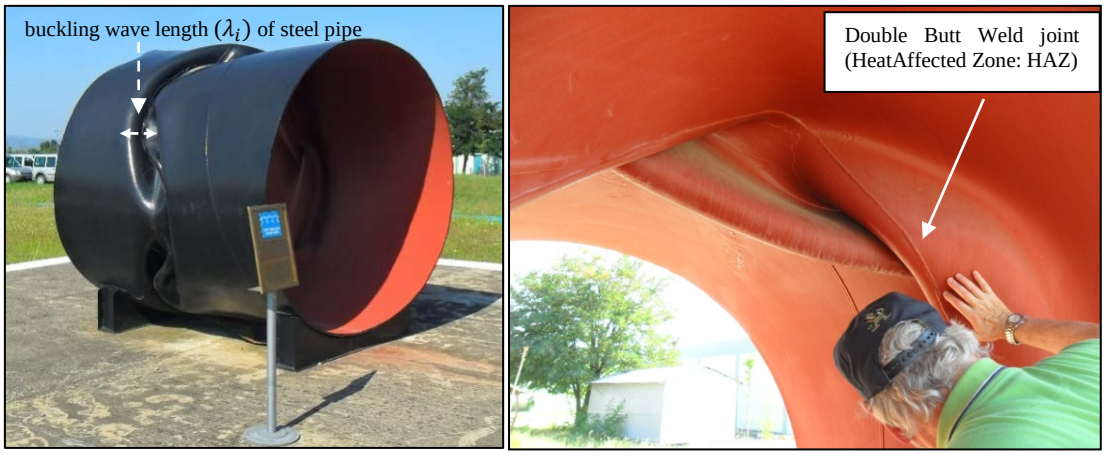

Fig. 4. *Damaged pipe under demonstration: General Directorate of ISU, Kocaeli (Photo: O'Rourke and E. Uckan)*

A close look to major wrinkle in Fig.4 indicates axisymmetric buckling without any welding failure. The axial displacement and rotation demands at buckle no. 1 and buckle no. 2 are reported to be 1.1 m and 0.5 m, and 8.1° and 8.5° [15], respectively. Results of the calculated axial displacement and hinge rotation demands at wrinkles are (1.1 m and 0.4 m) and (7.5° and8.0°), respectively, as presented in next section.

Damage due to the PGD hazard starts with local buckling of the pipe wall, followed by plastic strain accumulation at the wrinkling and fracture. The strain accumulated due to this additional deformation is a function of the local buckling wavelength of the pipe, and the magnitude of the deformation itself [23]. Based on bifurcation theory of elastic cylinders under axial compression [9], the following expression can be written to compute the wrinkle wavelength λ_i of a long tube:

$$\lambda_i = 3.44\sqrt{\frac{Dt}{2}} \tag{1}$$

The theoretical initial local buckle wavelength, from Eq. (1), is calculated to be 48 cm, which is reasonably consistent result with the field observations (Fig. 4), and the FE model (52 cm), where pipe diameter is D= 2.2 m, and wall thickness is t = 18 mm.

3. Analytical Beam on Elastic Foundation (BEF) Model

The separation distance between two wrinkles are calculated by using an analytical BEF model. A pair of wrinkle typically form as shown in Fig. 5. Much of the flexural demand due to transverse offset component is accommodated by abrupt rotation at each wrinkle. Whereas the longitudinal compression demand due to longitudinal offset component is accommodated by axial compression at each wrinkle. Herein the locations of the wrinkles due to transverse offset component of the fault are determined through an analytical formulation which is based on BEF model (Appendix.2).

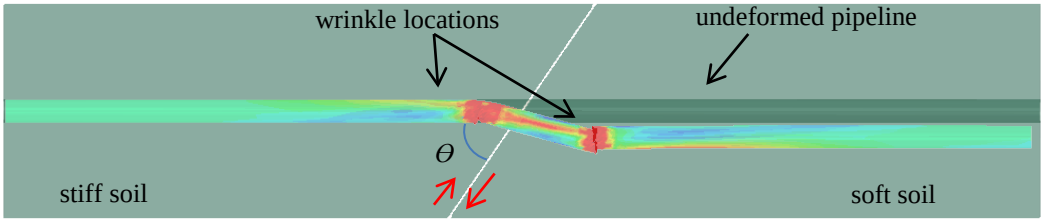

Fig. 5. *Damaged pipe and wrinkle locations under axial compression*

4.The 3D Finite Element Model

General purpose FE program, ABAQUS [25], is used to compute the response of pipe to incrementally applied fault displacements. The diameter of the pipe is D = 2200 mm, thickness is t =18 mm, total length of the FE model is 100.0 m (50.0 m at both side of fault), pipe burial depth (distance from the top of pipe to ground surface) is 1.5 m, depth and the widths of the trench are 5.0 m and 20.0 m, respectively, (Fig. 6). The steel is API Grade B steel with minimum specified yield stress of 241 MPa. The backfill material of the trench is a mixture of native soil (soft and stiff clay) with sand and gravel. The equivalent elastic module and cohesion for soft and stiff soils are assumed to be E = 8, 16 MPa and C = 20, 40 kPa, respectively. The fault width (gap) between the soil blocks is taken to be 30 cm as suggested by Vazouras [22].The model follows the same trends indicated in [22] and [26].

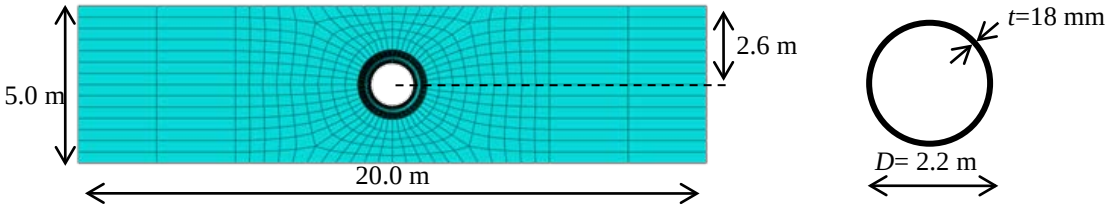

Fig. 6.*The FE mesh and cross sectional view of the soil-pipe interaction system*

The main difference between the Vazouras' studies [22] and [26], and current one can be stated as follows. In their study, a steel pipe which is subjected to net tension due to strike slip fault offset was analyzed. Whereas in the current study the pipe is subjected to net compression. Such a situation is not a desired option for steel pipes as it may lead compressive failure of pipe. Therefore, it should be avoided during design phase. Another difference is that, in reality the boundary conditions of the pipe is neither free nor fixed at both ends. In this study we also considered flexible boundary conditions (equivalent boundary springs) at the surface of pipe which is in between these two extreme cases. The properties of spring are calculated by simplified (analytical) expressions (Appendix.1).

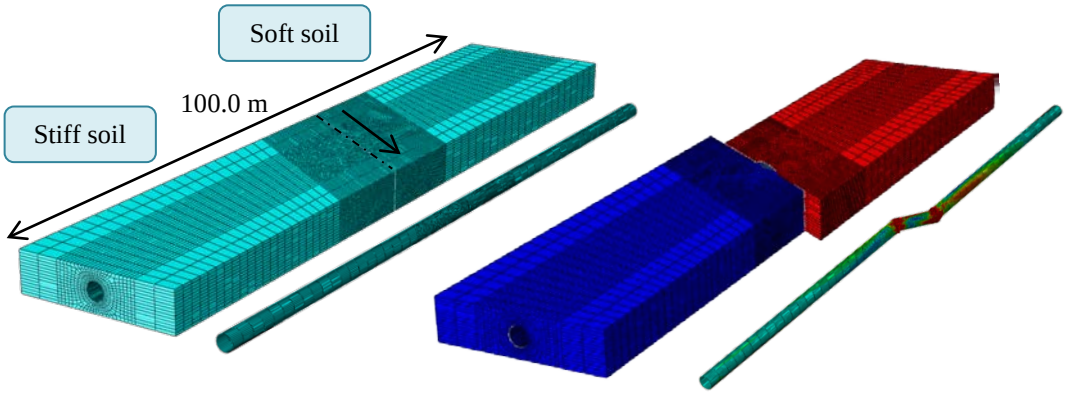

Fig. 7. *The 3D FE continuum soil-pipe model subjected to fault rupture*

The cross sectional view of the pipe and FE meshing of the pipe-soil model are shown in Fig. 7. The model consists of 53 000 solid elements and 5 000 shell elements. In order to reduce the computational time, the mesh size of the solid elements (soil) increases towards the boundaries. The model employed 8-node linear brick, reduced integration hour-glassing control (hexahedron-type C3D8R) with large deformations and nonlinear material model using Mohr-Coulomb yield model for soil elements; 4-node shell element (S4R) with reduced integration using isotropic Von Mises yield model for the steel pipe element.

A surface to surface contact algorithm is employed between the outer face of steel pipe and surrounding soil. The model allows separation between surfaces after contact occurs. Initially the friction coefficient between the surfaces is taken to be μ = 0.3 as provided in references [22] and [26]. Different boundary

conditions such as fixed, free and flexible end cases are considered. Nonlinear springs at the end of the pipeline are used to refine the finite element model.

5. Numerical analysis and results

A quasi-static nonlinear analysis of the pipe soil interaction system to incrementally applied fault displacements is performed. The loading is performed in three stages. Initially, geostatic loads are applied to calculate the stresses in the pipe due to the self-weight of the pipe and soil. In the second step, an internal pressure of 10 bar [15] is applied to the inner surface of the pipe wall. Finally, incremental fault displacements are applied to the block on the right hand side while keeping the other fixed. Pipe deformations and axial strains are calculated. The effects of pipe-end boundary conditions and internal pressure of pipe are investigated. Several analyses are performed to calculate the response of the pipe with different boundary conditions such as fixed, free and flexible pipe end connections.

5.1 Results for local buckling

Results of the 3D FE model including the effects of pipe internal pressure and fixed end boundary conditions are provided below for comparison with field investigations. The deformed shapes of the pipe and reduction of the pipe cross section are clearly observed in Fig.8 and 9. Based on the report provided by May 2001 Eidinger Report [15], the angle of rotation at each wrinkle is about 8° and the distance between hinges is 17.1 m.

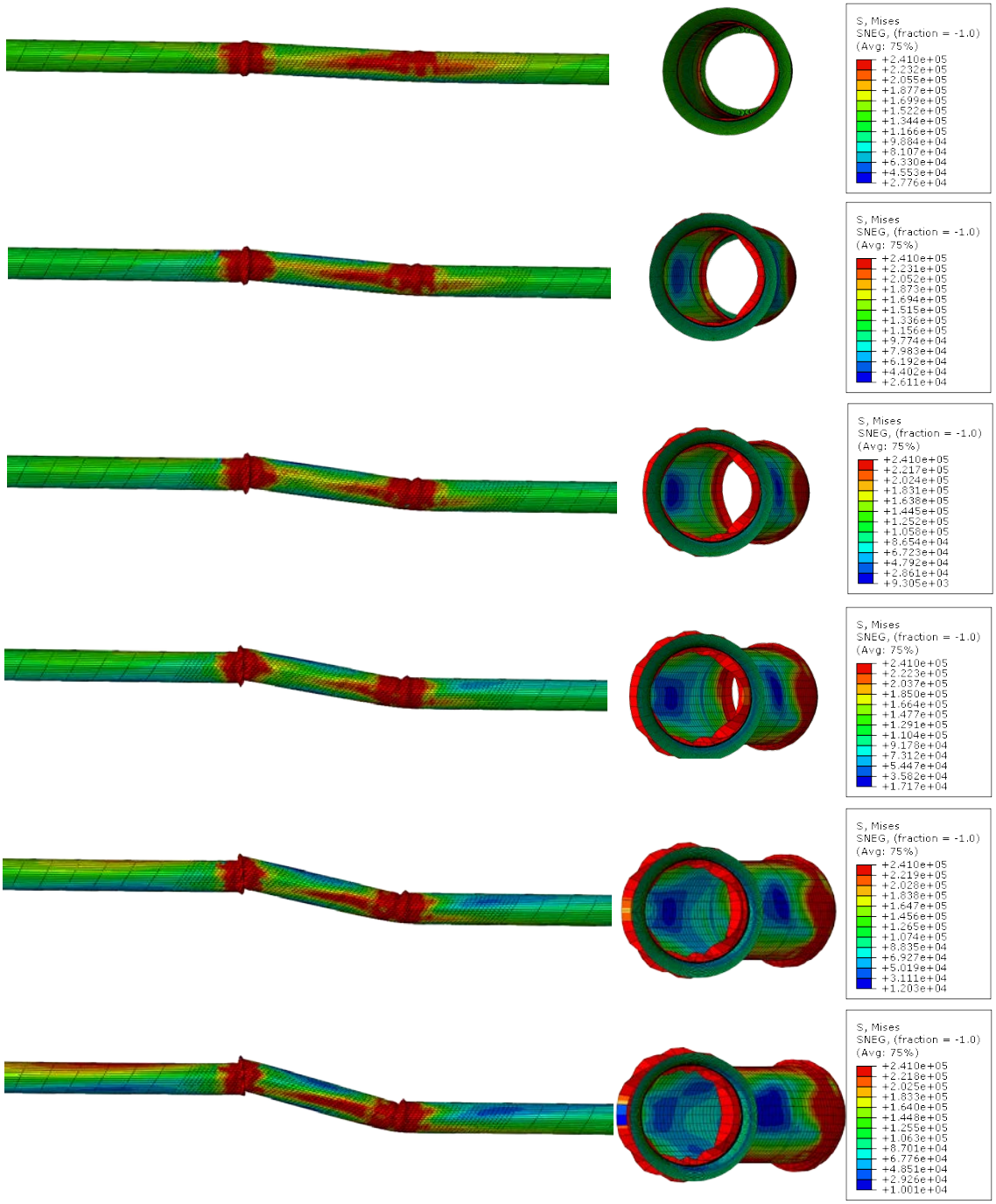

Fig. 8. *The Z-shaped deformation of pipe subjected to compressive strains at fault displacement increments of 0.5 m assuming fixed end BCs at pipe end and w/ internal pressure (10 Bars)*

Numerical results verify that the deformed Z-shape of the pipe and buckle distance is about 16.5 m for assuming the fixed end condition for the pipe. When the pipe-end is free, the separation distance increases to 21.0 m and axial strains decrease by an amount of 60%. The results of free end boundary conditions will be presented in the next section.

The deformed shapes of the pipe with internal pressure and fixed end conditions, are shown for various fault offset values in Fig.8 and 9.The lateral and axial components of the fault offset were 2.30 to 2.47 m and 1.7 m, respectively [15].

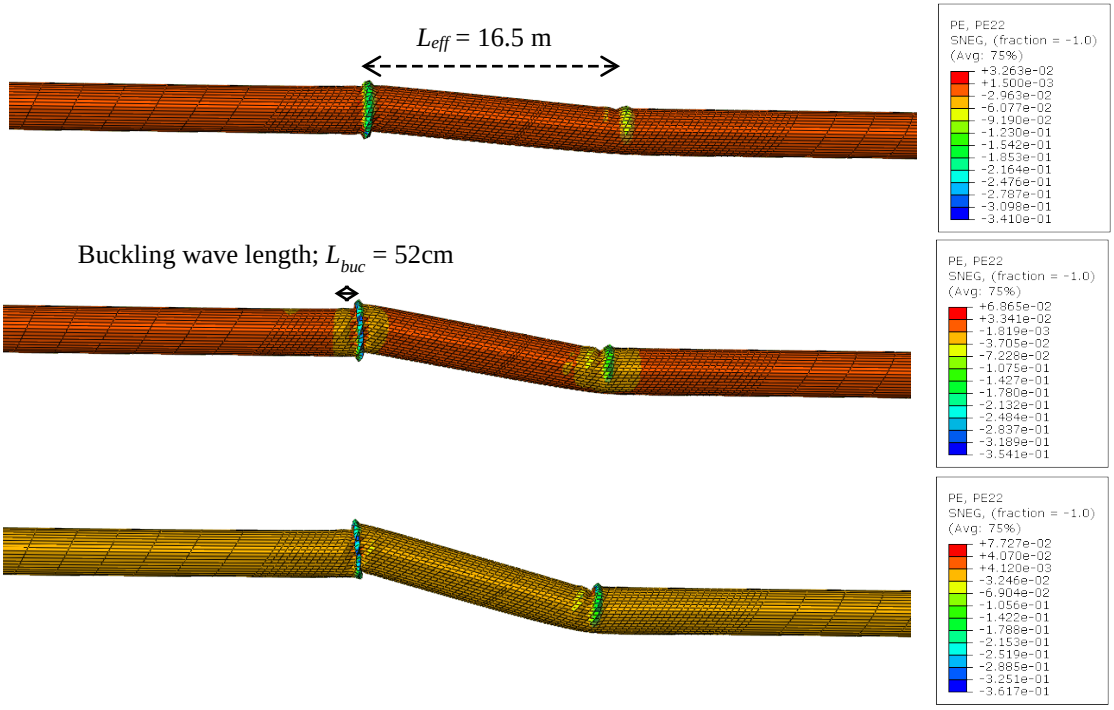

Fig. 9. *Deformed shapes of pipe (w/ internal pressure) and separation distance of wrinkles at fault displacements of 1.0,2.0, and 3.0 meters (fixed end BC) and internal pressure (10 Bars)*

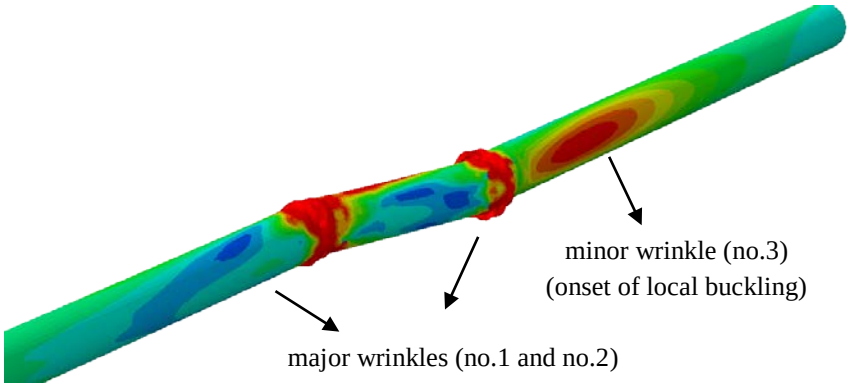

Fig. 10. *The initiation of third (minor) wrinkle at the onset of local buckling*

The onset of local buckling of pipe initiates when the axial strains due to bending and shortening exceeded that of the buckling strain of the pipe. The lower bound of the theoretical compressive stress for a non-pressurized cylinder to reach onset of wrinkling for a perfect cylinder having pipe wall thickness of t = 18 mm and radius of R = 1100 mm is provided by Eidinger equal to 0.29% [15]. The theoretical buckling strain considering internal pressure can be computed from Eq. (2) equal to0.4%. The 3rd wrinkle shown in Fig.10, which is at this stage of damage. The observed and calculated deformation of Thames water pipe are shown in Fig.11.

The calculated relative axial displacement and rotation demands at wrinkles (no.1 and no.2) are plotted with respect to the fault displacement in Fig.12. The major results from the numerical analyses are compared with the field measurements and provided in Table 1. The analyses results and field measurements seems to agree quite well. The maximum rotations and displacements on the soft and stiff

soils are 7.5° and 8°, and 1.1 m and 0.5 m, respectively. The relative displacement on both wrinkles are found different possibly because of assuming the boundary conditions as rigid and due to different soil properties.

In Eidinger's report [15], it is reported that the pipe axial force goes to zero at roughly 150 meters from the fault, hence a 300 m model would be required to represent the overall behavior of the pipe. In other words, 300 m FE model will be sufficient to model actual behavior of the pipe. On the other hand, in our case the pipe is modeled to be only 100 m long and the boundary condition is assumed to be rigid. The effects of free boundary conditions are elaborated in the next section. In a recent study conducted by Vazouras et al. [26] nonlinear boundary springs are provided at the two ends of the pipeline in a refined FE model.

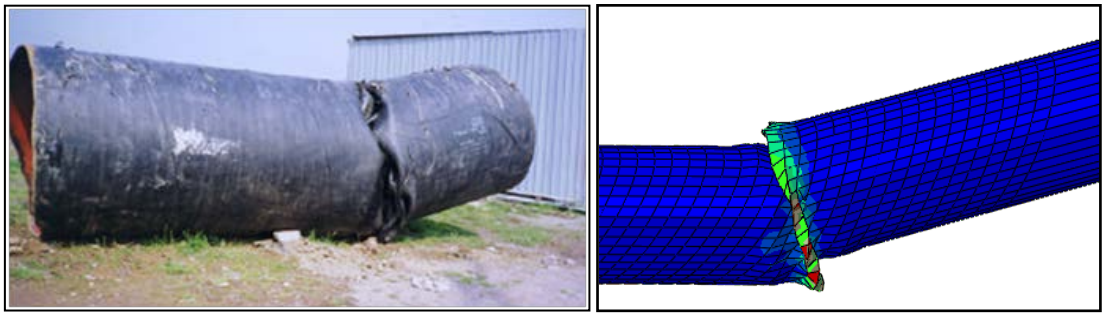

Fig. 11. *Permanent deformations of Thames water pipe (observed vs. calculated)*

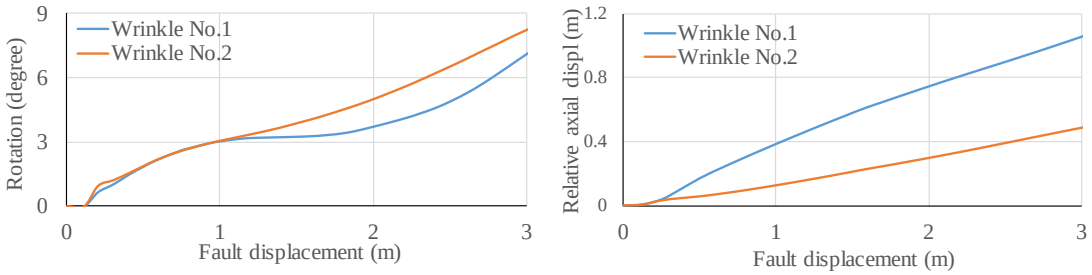

Fig. 12. *Displacement and rotation demands at major wrinkles 1 and 2 with respect to fault displacement*

Table 1 Comparison of numerical results and field measurements

	Separation distance between wrinkles (m)	Average axial strain at wrinkles(1&2)	Rotation demands at wrinkles (1& 2) (degrees)	Location of the 3rd minor wrinkle (m)	Local buckling wavelength (cm)	Local buckling strain (%)
Field observations	17.1-17.6	15 - 20%	7.5-8.5°	13.0	50-60	-
Numerical	16.5	15 - 20%	7.5-8.0°	13.1	50-55	0.21
Theoretical (Gresnigt)	-	-	-	-	48	0.19

5.2Effects of free boundary conditions

Boundary conditions (BC's) might have great influence on the performance of pipes. Two different types of BC's are considered. When the pipe end is assumed fixed, i.e. no slippage of pipe is allowed, higher strains are involved as compared to free end case (by 60%). Therefore, fault displacement at limit

condition is lower, indicating a more critical condition for pipe response. Results for the fix-end pipe have been presented in the previous section. This section includes the results for the pipe with free end.

When the pipe-end is free, slippage occurs in pipe. Assuming a free-end boundary conditions, the separation distance between wrinkles increase from 16.5 m to 21.0 m (about 25%), and pipe axial strains decrease as compared to fixed end case. The effects of boundary conditions on the pipe response are shown in Fig. 13-15.

According to Fig. 15, the amount of slippage is 1.5 m, which is very close to the axial shortening reported by Eidinger [15]. Observing the deformed shapes of pipes and strain accumulations at wrinkles (Fig. 9), it can be concluded that the fixed-end assumption represents better the real behavior of the Thames Water pipeline.

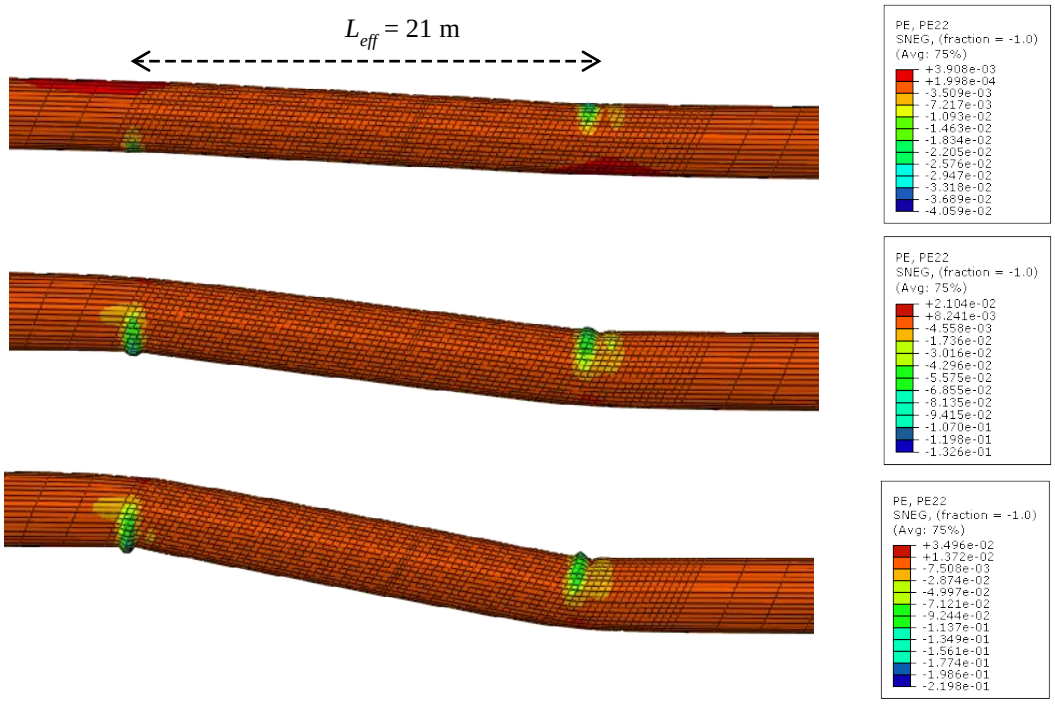

Fig. 13. *Deformed shapes of the pipe (w/ internal pressure) and separation distance of wrinkles at fault displacements of 1.0,2.0, and 3.0 meters (free end BC)*

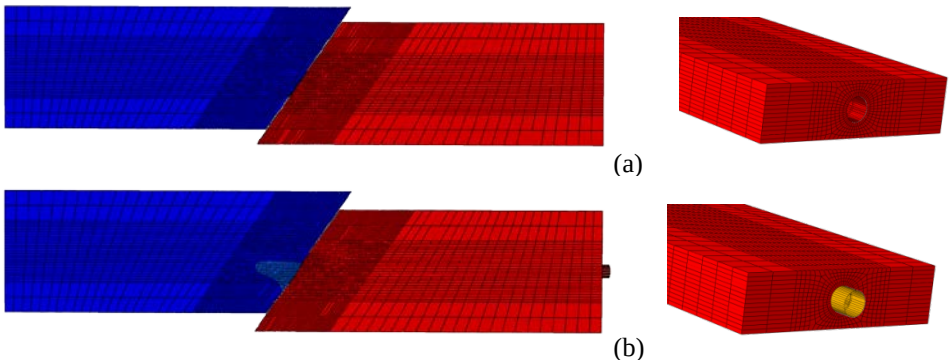

Fig. 14. *Effects of boundary conditions on the response of pipe a) fixed-endb) free-end (slippage allowed)*

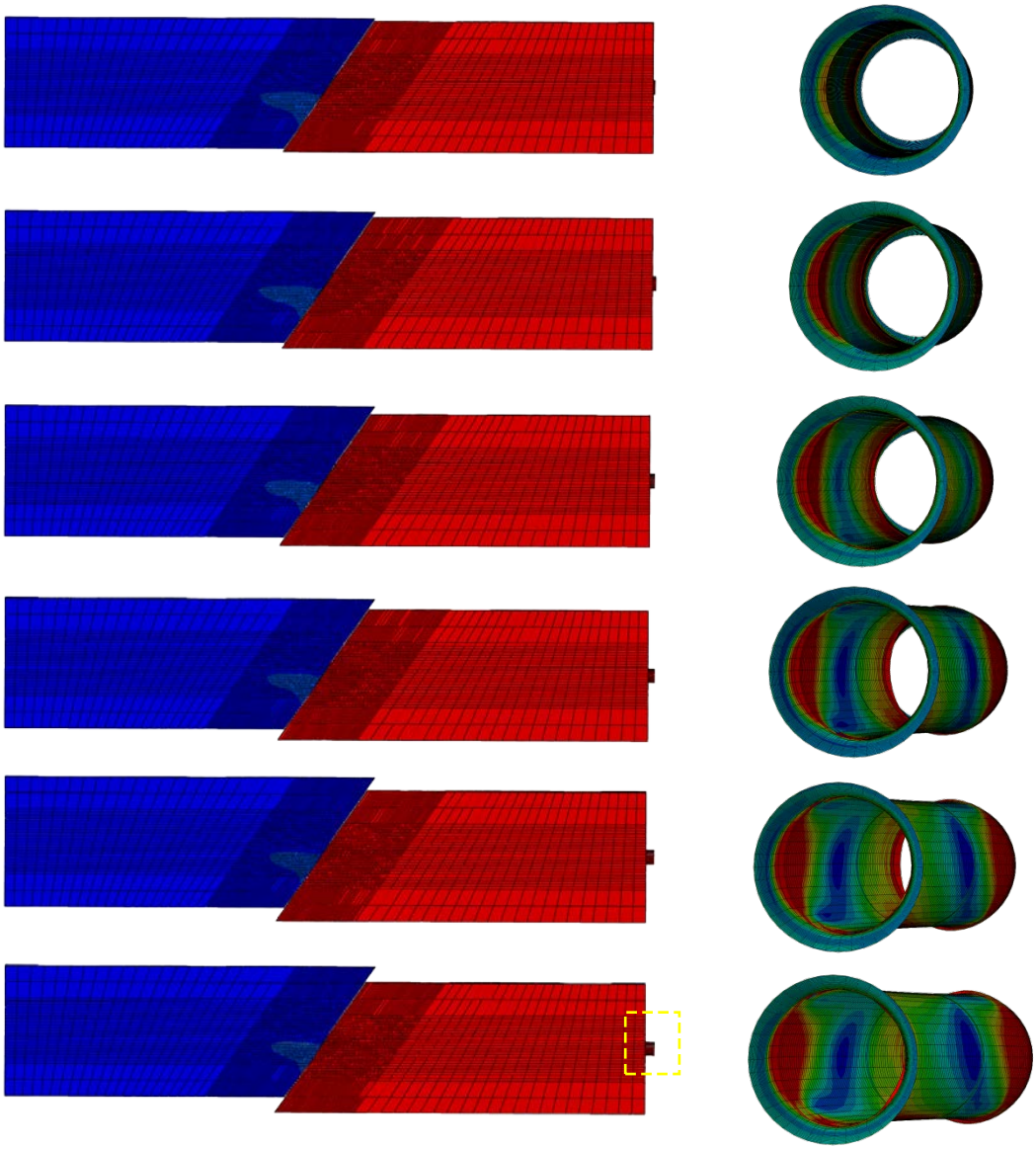

Fig. 15. *The slippage of pipe at free-end and deformed shapes of the pipe at various fault displacements*

It can be seen that the displacement and rotation demands at wrinkles are quite sensitive to the boundary conditions of the pipe. When the pipe end is assumed fixed, analysis results seem to agree better with field observations as compared to the free end case. However when equivalent boundary springs are used better results are obtained. A nonlinear soil spring (Fig. 16), is also employed at the pipe end surface with an approximate spring coefficient of 600kN/m. The parameters of the equivalent boundary springs for Thames Water Pipeline is provided in Appendix.1. The axial strain values of the pipe due to fault displacements of 1.0, 2.0 and 3.0 m are given In Fig. 17. It is also observed that, when the friction coefficient reduce the separation distance between wrinkles increase and consequently axial strains reduce.

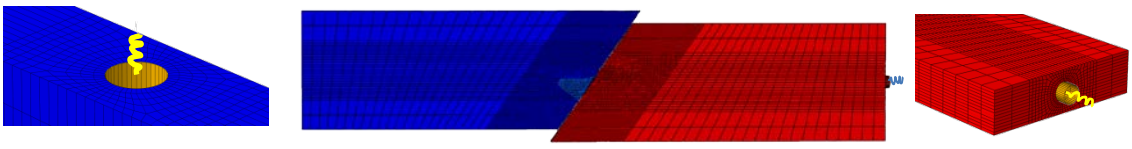

(a) (b)

Fig. 16. *Equivalent boundary spring model at fault displacements of a) 0.0 and b) 3.0 meters*

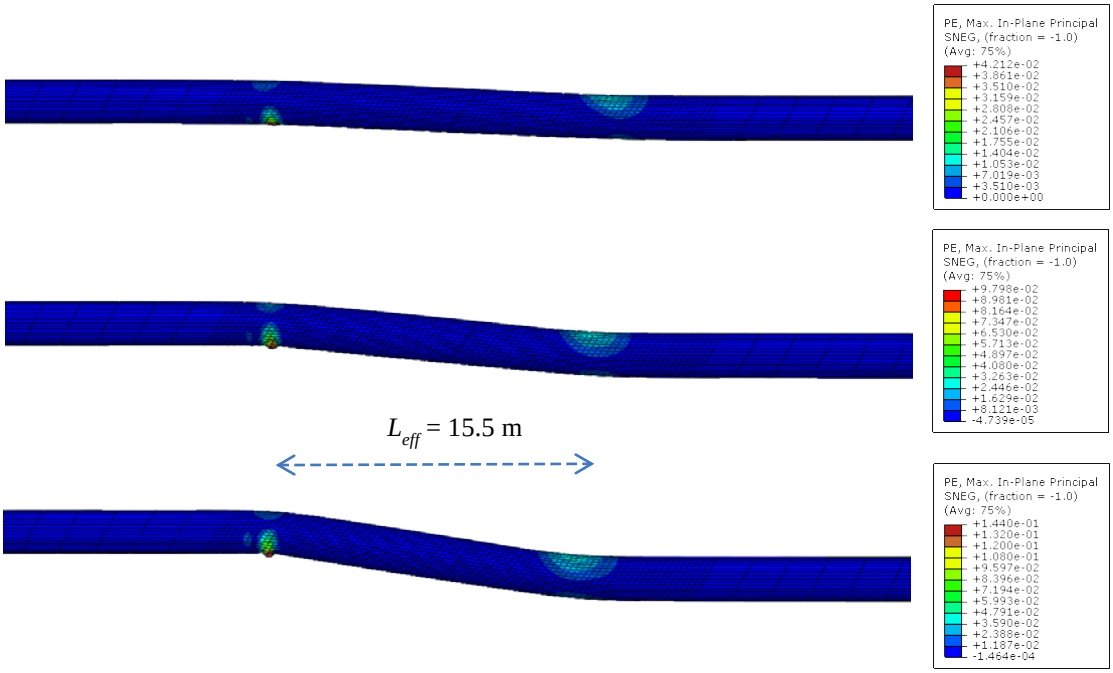

Fig. 17*. Equivalent boundary spring model at fault displacements of 1.0, 2.0 and 3.0 meters*

5.3Effects of internal pressure

Internal pressure provides additional stiffness against cross-sectional distortion and ovalization, delays local buckling initiation and increases the corresponding critical axial compressive strain, associated with local buckling. Therefore, it is considered beneficial for pipe response. Due to internal pressure, transverse or hoop tensile strain are developed. Gresnigt [27] proposed an empirical equation to include this effect, which was shown to have good agreement with his experimental results.

$$\varepsilon_{cr} = 0.5\frac{t}{D} - 0.0025 + 3{,}000\left[\frac{D(P_i - P_e)}{2tE}\right]^2 \qquad (2)$$

where P_i is the internal pressure, assumed to be larger than the external pressure P_e, and E is the elastic modulus of steel. Substituting the internal pressure of 10 bar into Eq. (2) the critical buckling strain is calculated to be, ε_b =0.4% which is very close to the calculated value of 0.6% at the onset of local buckling.

Local buckling at both wrinkles occurs nearly simultaneously at the very early stage of fault displacement (at 15 cm of fault displacement). As fault rupture increases most deformation (rotation and displacement) localizes and takes place at the wrinkle location.

The deformed shapes of the pipe with and without internal pressure are shown in Fig. 18. It is seen that internal pressure increases the stiffness of the pipe and changes the buckling mode from inwards to outwards. The post buckling behavior of the pressurized pipe with fixed end boundary condition in (a) is consistent with the observed buckled shape of Thames Water pipeline.

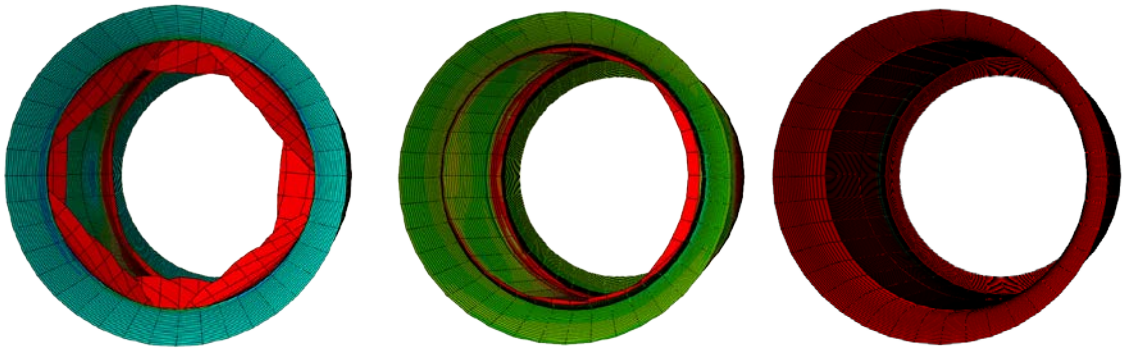

Fig. 18. *Deformed shapes of pipe for (a) w/o internal pressure (fixed end),(b) w/ internal pressure (fixed end) and (c) w/ internal pressure (free-end) cases, at fault displacement of 0.5m*

5.4 Effects of soil properties

The backfill material of the trench was a mixture of native soil with sand and gravel. Originally the soil properties at both sides of the fault line were different (soft and stiff clay). Therefore, wrinkle locations were unsymmetrical with respect to the fault line

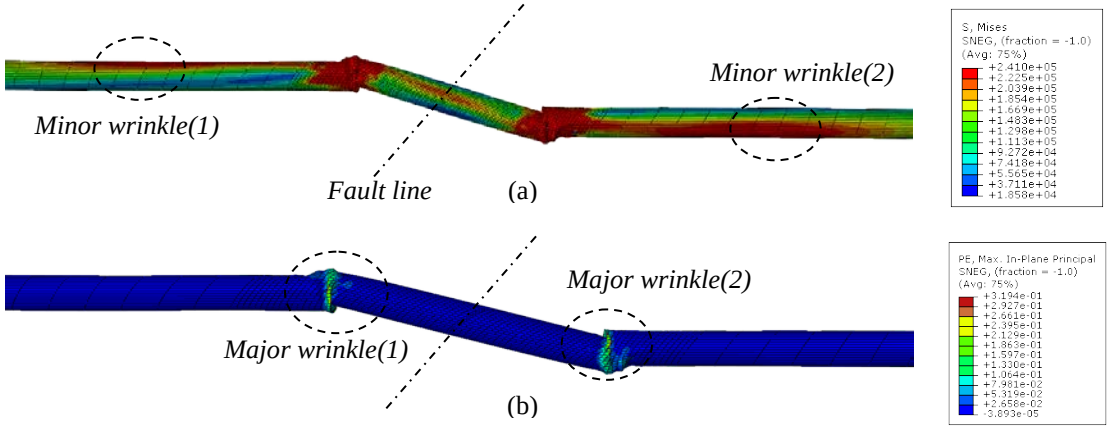

Fig. 19. *Deformed shapes of pipe under homogenous soil properties (a) symmetrically located wrinkles with respect to the fault line, (b) axial strain values*

In this study we also investigated the effects of homogenous soil properties on the formation of wrinkles along the pipe. It is observed that for an equivalent elastic module of E = 10 MPa and cohesion of C = 5 kPa, the locations of both major and minor wrinkles tend to happen symmetrically with respect to the fault line (Fig.19), indicating that the soil-pipe interaction model is quite sensitive to the properties of the surrounding soil. This comparison has been made for pipe operation pressure of 10 bars and fixed end pipe conditions.

6. Performance criteria for high quality steel pipes

In the 2001 American Lifelines Alliance (ALA) guidelines [28] and the 2004 Pipeline Research Council International (PRCI) guidelines for Gas and Liquid Hydrocarbon Pipelines [29], the tensile rupture strain capacities for modern pipelines with high-quality overmatched welds are associated with defined performance goals [5].
For pipelines where the performance goal is to maintain pressure integrity, the tensile strain limit is 4% in the ALA guideline and 2–4% in the PRCI guideline. If the performance goal is immediate operability such that post-event functionality of the pipe is expected, the ALA strain limit is 2%, while the PRCI limit is 1–2%. However, these tensile strain limits are well beyond the elastic range of pipe material, and require appropriate qualification process.

The limit state of compressive strength is associated with local buckling and depends on pipe geometry, material, initial imperfections and the level of internal pressure. The failure process begins with wrinkle initiation, followed by wrinkle growth (e.g., 5% internal diameter loss), folding of pipe at the wrinkled area and ultimately rupture of the pipe wall. However, for the performance goal of post-event operability, the literature suggests using the onset of wrinkling as the appropriate limit state.

When the pipe is subjected to compressive loads (which is the case of Thames Water Pipe) limit states of pipe are expressed as a function of diameter to thickness (D/t) ratio of pipe. Wijewickreme, (2006) provided following limit states for compression controlled ruptures;

For 10 % prob. of failure, Axial strain (ε_1) = 0.4 t/D = 0.33 % (3)
For 90 % prob. of failure, Axial strain (ε_2) =2.4 t/D = 2 % (4)

By applying these expression to our case study (t/D =0.0082) we obtain axial strains of ,

(ε_1) = 0.4 t/D = 0.33 % (5)
(ε_2) =2.4 t/D = 2 % (6)

When comparing these limit states to the observed pipe strain (According to the Eq. 3-6), it can be said that the induced strain is far beyond the limit values (about 10 fold) provided by codes. Therefore, pipe would definitely fail and it did. Surprisingly, tearing of the pipe wall was observed only at a single or two points, possibly because of half cycle loading of the fault offset. Had the loading be reversal the damage could have been more intense.

7. Conclusions

The failure analysis of a steel pipeline subjected to 3.0 m of compressive right lateral strike slip fault is simulated by a 3D nonlinear continuum finite element approach. The behavior of pipe subjected to monotonic static loading due to fault rupture is studied. The transition from initial local buckling at the pipe wall (no loss of pressure containment) to rupture of the pipe wall at wrinkles (loss of pressure containment) is investigated.

Distance of the buckles, axial and rotational demands at wrinkles and buckling wave length of the pipe (wrinkle) are computed and compared with previous reported results and field observations. Results revealed that behavior of pipes under compressive strains in large plastic strains is quite complex and very sensitive to the pipe end conditions, internal pressure and properties of soil backfill material.

The Kullar test site provided valuable information regarding the behavior of buried steel pipes subjected to compressive strike slip faults. Main outcomes of the research are:

1) The 3D model can reasonably estimate the location of wrinkles and hinge separation distance. The first and second wrinkles occur at both side of the fault line and third (minor one) in the soft soil region. The separation distance of the major wrinkles is 16.5 m which is compatible with observations (17.1m).

2) Soil properties were different at both side of the fault line. Therefore, the locations of wrinkles were unsymmetrical with respect to the fault, one close to the fault line on the stiff side away from the fault line, in the soft soil region. As for homogenous soil properties with respect to the fault line, it is seen that wrinkles occur symmetrically with respect to the fault line. It can be concluded that the response of the soil-pipe interaction system is quite sensitive to the properties of the surrounding soil as well as the contact conditions at the pipe soil interface. Small changes in such properties may lead big changes in pipe response.
3) The end conditions of pipe play important role in the response of pipe. When pipe-slippage is permitted (i.e. free end), the separation distance between wrinkles increase (up to 25%) and pipe axial strains reduce as compared to the fixed-end case. The amount of outwards slippage of the pipe in the free end condition is found to be 1.5m, which is very close to reported axial shortening of 1.7 m.
4) Tolerable fault displacement at the limit state of the fixed-end pipe is much lower than the one with free-end, therefore indicates a critical condition for pipe. It is suggested that if the BC's of the pipe is not known, fixed end case should be considered for a conservative pipe design.
5) Fault displacement at the onset of local buckling was very low, about 12-15 cm for the Thames Pipeline. When the fault displacement reaches the critical buckling strain all rotation and displacement demand concentrate at wrinkle, while the strain in the rest of the pipe remains constant.
6) The pipe wall at wrinkles is folded into the pipe. As a result, the diameter of the pipe reduced from 2.2 m to 1.4 m. The 3D models captured the complex post buckling modes of pipe.
7) The average axial strain and rotations at wrinkles are (10-20%) and 8.5 degrees, respectively which are compatible with findings of previous field observations and researches.
8) Internal pressure delays and shifts the buckling mode from inwards to outwards and delays local buckling formation. Therefore, can be considered beneficial, as noted in previous works.

For design purposes a simplified model is required to represent the post elastic behavior of the pipe under net compressive loads. Authors are also working on the development of a semi-empirical model that calculates displacement and rotation demands causing leakage (tearing of the pipe wall), and can be used for the assessment and design of buried steel pipes subjected to compressive fault displacements.

Acknowledgements

The General directorate of Municipality of Kocaeli, Water and Sewage System (ISU) Mr. Ilhan Bayram and technical staff of ISU are gratefully acknowledged.

Appendix.1. Equivalent Axial Spring Stiffness at the end of Buried Pipe Model

It is possible to easily determine equivalent axial spring stiffness at the end of the pipe under strike-slip fault movement resulting in compressive strains.

Assume that, pipe is linear elastic and Axial rigidity is *EA* (*A*, is the area of cross section and *E* is the Young's modulus). Soil axial resistance constant is equal to f_m.

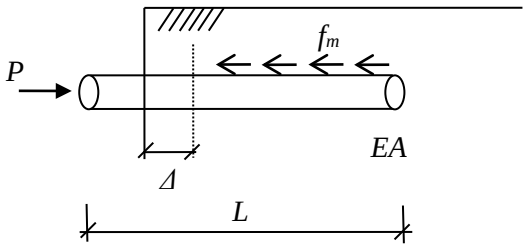

Fig. 20. *Buried pipe under applied axial load*

For applied axial load *P*, the length over which the soil axial resistance acts is;

$$L = \frac{P}{f_m} \tag{7}$$

The axial force in pipe;

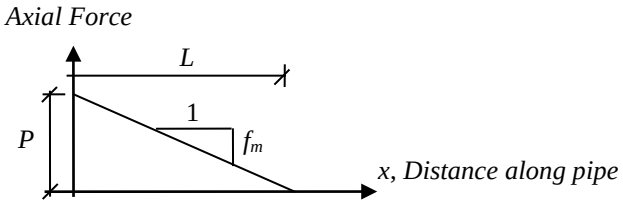

Fig. 21. *Axial force in pipe*

The axial strain in pipe;

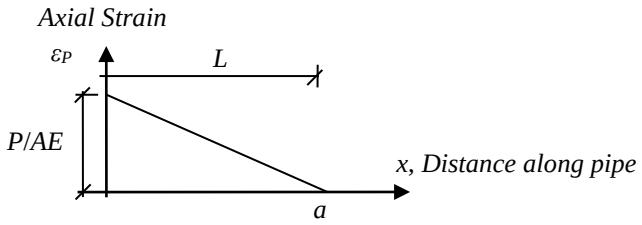

Fig. 22. *Axial strain in pipe*

$$\varepsilon_P(x) = \frac{P}{AE}\frac{(L-x)}{L} \tag{8}$$

Deformation at the end of model (i.e. *x* = a)

$$\Delta = \int_{\Delta}^{L} \varepsilon_P(x)dx = "Area" \; under \; "\varepsilon_P(x)" \; vs. "x \; curve" \tag{9}$$

$$\Delta = \frac{1}{2} \; L \; \frac{P}{AE} \; = \; \frac{PL}{2AE} \tag{10}$$

or

$$\Delta = \; \frac{P.P/f_m}{2AE} \; = \; \frac{P^2}{2f_mAE} \tag{11}$$

Equivalent spring stiffness becomes,

$$K \; = \frac{P}{\Delta} \; = \; \frac{P}{P^2/2f_mAE} \tag{12}$$

$$K \; = \; \frac{2f_mAE}{P} \tag{13}$$

$$K \; = \; \frac{2f_mAE}{P} \tag{14}$$

$$\frac{K}{f_m} = \frac{2AE}{P} \tag{15}$$

but

$$\frac{P}{AE} = \varepsilon_P \qquad (reasonablerange\ 0.0\ to\ 0.001) \tag{16}$$

Table 2 Equivalent spring stiffness values

P/AE	0.00001	0.00002	0.00005	0.00010	0.00020	0.00050	0.00100
***K/f*$_m$**	200.000	100.000	40.000	20.000	10.000	4.000	2.000

For known pipe and soil properties, *AE* and f_m is easy to determine. Table 2 can also be used to input spring stiffness values. Following charts are prepared for the known values of Thames Water Pipeline case where, Young's Module E is, 210 Gpa (210,*10^6kN/m^2), thickness of pipe is *t*, 18 mm, diameter D is, 2.2 meter, internal pressure is 10 Bar (1000 kN/m^2) , Axial rigidity is *EA* 26*10^6kN, and f_m is 300 kN/m.

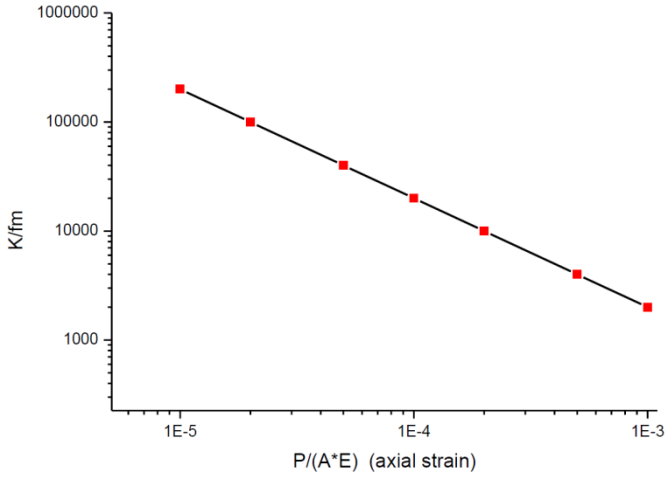

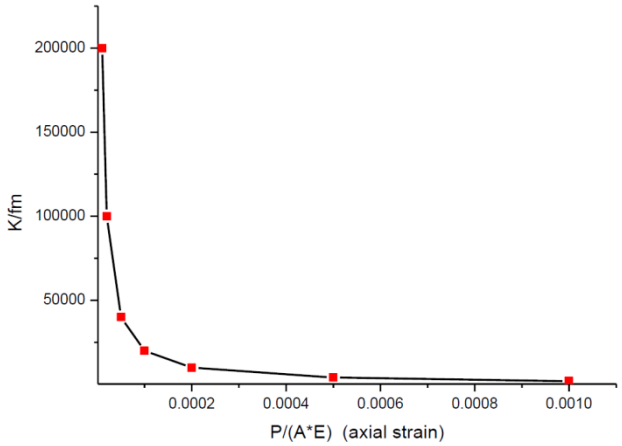

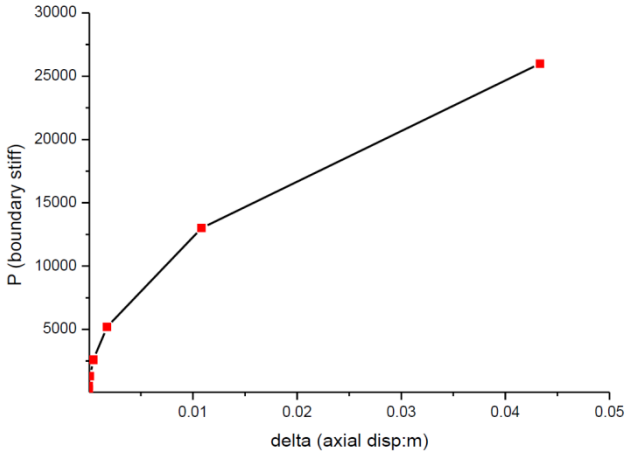

Fig. 23. *Equivalent axial spring coefficient*

Appendix.2. Calculation of the Separation Distance between wrinkles by using an Analytical Beam on Elastic Foundation (BEF) model

It is assumed that the wrinkle develops at the location where the bending moment in the pipe is a maximum and there is a point of outer flection (in flection point) at the fault. For the solution of BEF problem, Volterra and Gaines [24] suggest a long beam which is subjected at the extremity $x = 0$ to a vertical force P and to a couple M, as shown in Fig. 24.

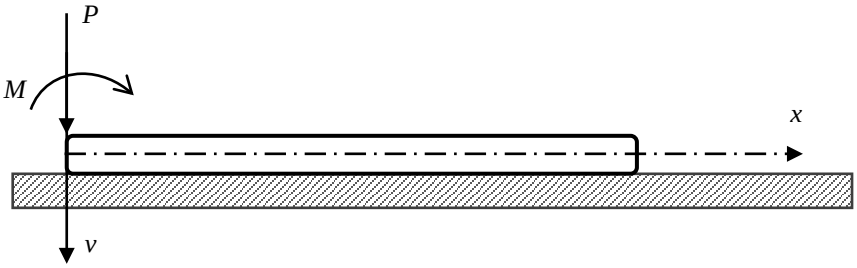

Fig. 24. *Beam on Elastic Foundation*

The deflection and rotation of the beam at $x = 0$ can be calculated as follow for $x = \infty$, $v = M = 0$, and $C_1 = C_2 = 0$.

$$v = e^{-\alpha x}[C_3 \sin \alpha x + C_4 \cos \alpha x] \tag{17}$$

The two constants C_3 and C_4 of Eq. (2) are determined from the boundary conditions at $x = 0$.

$$EI\frac{d^2v}{dx^2} = -M \tag{18}$$

$$EI\frac{d^3v}{dx^3} = -V = P \tag{19}$$

It follows that

$$C_3 = \frac{M}{2\alpha^2 EI} \tag{20}$$

$$C_4 = \frac{P-\alpha M}{2\alpha^3 EI} \tag{21}$$

and the deflection curve becomes

$$v = \frac{e^{-\alpha x}}{2\alpha^3 EI}[\alpha M \sin \alpha x + (P - \alpha M)\cos \alpha x] \quad (22)$$

while the slope equation is

$$\theta = \frac{dv}{dx} = -\frac{e^{-\alpha x}}{2\alpha^2 EI}[P \sin \alpha x + (P - 2\alpha M)\cos \alpha x] \quad (23)$$

an the extremity $x = 0$ of the beam, one obtains

$$v = \frac{P - \alpha M}{2\alpha^3 EI} \quad (24)$$

$$\theta = \frac{P - 2\alpha M}{2\alpha^2 EI} \quad (25)$$

For our case M(0) = 0 = M,

$C_3 = 0$

$C_4 = \frac{P}{2\alpha^3 EI} = \sqrt{0}$

But for the case where the pipe is symmetric with response to the fault

$\sqrt{0} = \frac{\Delta T}{2}$

where ΔT is the transverse component of the of the fault offset

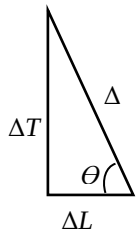

$$\Delta T = \Delta \sin\Theta \quad (26)$$

We also have in general,

$$M(x) = -EI\frac{d^2v}{dx^2} \quad (27)$$

$$\frac{d^2v}{dx^2} = 2\alpha^2 e^{\alpha x}(-C_2 \sin \alpha x + C_1 \cos \alpha x) + 2\alpha^2 e^{-\alpha x}(C_4 \sin \alpha x - C_3 \cos \alpha x) \quad (28)$$

for our case

$$M(x) = -EI2\alpha^2 e^{-\alpha x}(\frac{\Delta T}{2} sin\alpha x) \quad (29)$$

$$M(x) = -EI\alpha^2 \Delta T e^{-\alpha x} sin\alpha x \quad (30)$$

$$M(x) = \gamma e^{-\alpha x} sin\alpha x \quad (31)$$

We want the location x_{max} where M is x maximum, that is where dM/dx = 0.

$$\frac{dM}{dx} = \gamma e^{-\alpha x} cos\alpha x\alpha + \gamma sinx e^{-\alpha x}(-\alpha) = \gamma e^{-\alpha x}\alpha(cosx - sinx) = 0 \quad (32)$$

Cosαx = sinαx hence αx is equal to π/4

$$x_{max} = \pi/4\alpha \quad (32)$$

again in general,

$$\alpha^4 = \frac{\beta}{4EI} \quad (33)$$

Hence for our case

$$x_{max} = \frac{\pi}{4\sqrt[4]{\frac{\beta}{4EI}}} \quad (34)$$

$$\beta = \frac{P_u}{D} \quad (35)$$

For the Kullar Pipeline, Eidinger report [15] present a number or estimate for the transverse (horizontal) soil spring.

Model P1.1 (Model P1.1, "P" = Production, 1.1 = model number , revision 1, represents the case with soil properties based on in-situ tests with lower bound properties)

$P_u = S_u * N_{ch} * D_{outside}$= 47.880 (kN/m^2) * 6 * 2.236 (m) = 642.37 kN/m $\beta = P_u / D$ = 287.285kN/m^2

where N_{ch} = 5.5 to 6 (say 6) from Figure 5.7b of ASCE 1984 [21], with 2.236 m of diameter of pipe, and the undrained shear strenght of the alluvial clay is assumed to be S_u = 47.880 kN/m^2.

Model P1.2 (Model P1.2 is the same as Model P1.1, but soil properties based on in-situ tests with upper bound properties.) It is assumed that the undrained shear strenght of the clay is S_u = 95.760 kN/m^2

P_u= 1284.716 kN/m $\beta = P_u / D$ = 574.57 kN/m^2

Model P1.3 (Model P1.3 examies the first issue by adjusting the soil springs to reflect a reduced amount of cover over the pipelines at the fault crossing area. In Model P1.1 and P1.2, the cover was assumed to be in the average range possible which is about 1.775 m. For Model P1.3, it was assumed to be the minimum, or 1.35 m.)

P_u = 47.880 (kN/m^2) * 4.5 * 2.236 (m) = 481.769 kN/m and β = 215.46 kN/m^2

Model P1.4 (Model P1.4 is developed to account for the assymmetric pattern of soil properties along the lenght of the pipeline, as well as the observed asymmetric location of pipe wrinkles around fault crossing. Model P1.4 adopts the same assumptions as Model P1.3, with the following changes for soil properties. For transverse soil springs north of the observed fault offset location, use 50% of the soil spring values in P1.3.)

P_u = [47.880 (kN/m^2) * 4.5 * 2.236 (m)] / 2 = 240.884 kN/m and β = 107.73 kN/m^2

Pipeline

R = 1.118(m), D = 2*(1.118) = 2.236 (m)

t = 18 (mm) = 0.018 (m)

E = 200 GPa = 200,000,000 kN/m^2

$I = \pi t d^3/8 = \pi(0.018)2.236^3/8$ = 0.07527 m^4

$\sqrt[4]{\frac{\beta}{4EI}} = \left(\frac{287.285}{4(200{,}000{,}000)0.07527}\right)^{1/4}$ = 0.046736 1/m

$\left(\frac{574.57}{4(200{,}000{,}000)0.07527}\right)^{1/4}$ = 0.0555 1/m

$\left(\frac{215.46}{4(200{,}000{,}000)0.07527}\right)^{1/4}$ = 0.0435 1/m

$\left(\frac{107.73}{4(200{,}000{,}000)0.07527}\right)^{1/4}$ = 0.0365 1/m

$$x_{max} = \frac{\pi}{4\sqrt[4]{\frac{\beta}{4EI}}}$$

For β = 287.285

$\sqrt[4]{\frac{\beta}{4EI}}$=0.0467 (1/m) and x_{max}= 16.9 m.

β(kN/m^2)	$\sqrt[4]{\frac{\beta}{4EI}}$ (1/m)	Xmax (m)
287.285	0.0467	16.9
574.57	0.0555	14.2
215.46	0.0435	18.1
107.73	0.0365	21.4

In our analyses the separation distance between wrinkles is found as 17.1 to 17.6 m which is quite close to the value (16.9 m) which is provided by hand calculations.

References

[1] O'Rourke M and Liu X (2011) Seismic Design of Buried and Offshore Pipelines, MCEER-12-MN04.

[2] Uckan E, Akbas B, Kaya ES, Cakir F, Ipek C, Makaraci M, Ataoglu S (2016) Design Issues of Buried Pipelines at Permanent Ground Deformation Zones. Disaster Science and Engineering, Vol. 2, No. 2, pp. 53-58.

[3] Uckan E (2013) Lifeline damage caused in the 23 October (Mw=7.2) 2011 and 9 November (Mw=5.6) 2011, Van Earthquakes in Eastern Turkey. International efforts in lifeline earthquake engineering, technical council on lifeline earthquake engineering, monograph no:38, ASCE Edited by: Davis C, Miyajima M, Yan L.

[4] Akbas B, O'Rourke MJ, Uckan E, Shen J, Caglar M (2015) Performance-based design of buried steel pipes at fault crossings. In Proceedings of the ASME 2015 pressure and vessels & piping conference, PVP July 19–23, Boston, MA, USA.

[5] Vazouras, P., Karamanos, S. A., and Dakoulas, P. (2012), “Mechanical Behaviour of Buried Steel Pipelines Under Strike-Slip and Normal/Reverse Fault Displacements”, *Soil Dynamics and Earthquake Engineering*, Vol. 41, pp. 164-180.

[6] Uckan E, Akbas B, Shen J, Rou W, Paolacci F, O’Rourke MJ (2015) A simplified Analysis model for determining the seismic response of buried steel pipes at strike-slip fault crossings. Soil Dynamics and Earthquake Engineering, 75, 55-65.

[7] Reid SR (1993) Plastic deformation mechanism in axially compressed metal tubes used as impact energy absorbers. International Journal of Mechanical Sciences. (35)12, 1035-1052.

[8] Tutuncu, I. (2001), “Compressive Load and Buckling Response of Steel Pipelines during Earthquakes”, *Ph.D. dissertation, Cornell University*, Ithaca, NY.

[9] Bardi, F.C., Kyriakides, S., Plastic buckling of circula rtubes under axial compression-part I: Experiments, International J. Of Mechanical Sciences, Volume 48, Issue 8, August 2006, Pages 830-841.

[10] Kyriakides, S., Ju, G.T, 1992. "Bifurcation and Localization Instabilities in Cylindrical Shells Under Bending-I. Experiments", *International Journal of SolidsStructures*, Vol. 29, pp. 1117-1142.

[11] Karamanos, S. A., Tassoulas, J. L., 1996. "Tubular Members II: Local Buckling and Experimental Verification.", *Journal of Engineering Mechanics*, Vol. 122, pp.72-78.

[12] Chatzopoulou, G., Sarvanis, G. C., Papadaki, C. I., Karamanos, S. A., “Modeling of Spiral-Welded Pipe Manufacturing and its Effect on Pipeline Structural Performance”, *26th International Ocean and Polar Engineering Conference*, TPC-0226, ISOPE, Rhodos, Greece.

[13] Yun, H., Kyriakides, S., (1990) “On the beam and shell modes of buckling of buried pipelines”, *Soil Dynamics and Earthquake Engineering*, 9 (4), pp. 179-193.

[14] Eidinger JM, O’Rourke MJ and Bachhuber J (2002) Performance of a pipeline at a fault crossing. Seventh U.S. National Conference on Earthquake Engineering (7NCEE), Boston, Massachussets, EERI-2002-07.

[15] Eidinger, J (2001) Performance of Thames Water 2.2 Meter Diameter Pipeline at North Anatolian Fault Crossing. G&E Engineering Systems Inc. Report No. 48.01.01, prepared for Rennselaer Polytechnic Institute, National Science Foundation, May 9.

[16] Parker G (2000) The Effect of the 17 August 1999 Izmit Earthquake on the Izmit Water Supply Scheme. IBC 4th Annual Conference on Onshore Pipelines, Paris, 12-13 October.

[17] Tang A (2000)Izmit (Kocaeli) Earthquake of August 17, 1999, Including Duzce Earthquake of November 12, 1999 – Lifeline Performance, American Society of Civil Engineers, Technical Council on Lifeline Earthquake Engineering, Monograph No. 17.

[18] Liu A, Takada S and He Q (2014) The Failure Performance of Thames Water Pipeline at Fault Crossing in Kocaeli Earthquake, Second European Conference on Earthquake Engineering and Seismology, Istanbul, Aug 25-29.

[19] Takada S, Hassani N, Fukuda KA (2001) New proposal for simplified design of buried steel pipes crossing active faults. Earthquake Engineering and Structural Dynamics, 30, 1243-57.

[20] Liu A, Takada S, and Hu Y (2004) A Shell Model with an Equivalent Boundary for Buried Pipelines Under the Fault Movement, 13th World Conference on Earthquake Engineering (13WCEE), Vancouver, B.C., Canada, August 1-6, Paper No. 613.

[21] ASCE (1984) Guidelines for the seismic design of oil and gas pipeline systems. Committee on gas and liquid fuel lifelines, technical council on lifeline earthquake engineering. American society of civil engineers, ASCE, New York.

[22] Vazouras P, Karamanos SA, Dakoulas PD (2010) Finite element analysis of buried steel pipelines under strike-slip fault displacements. Soil Dynamics and Earthquake Engineering, 30, 1361-76.

[23] Fell BV and O'Rourke MJ (2014) Loss of Pressure Boundary through Buckling-Induced Fracture in the Ciudad Nezahualcoyotl Pipeline, Journal of Pipeline Systems Engineering and Practice 5(4).

[24] Volterra E and Gaines JH (1971) Advanced Strength of Materials, Civil engineering and engineering mechanics series, Prentice Hall.

[25] ABAQUS Version 6.13, Documentation Collection.

[26] Vazouras P, Dakoulas PD, Karamanos SA (2015) Pipe-soil interaction and pipeline performance under strike-slip fault movement. Soil Dynamics and Earthquake Engineering, 72, 48-65.

[27] Gresnigt AM (1986) Plastic Design of Buried Steel Pipelines in Settlement Areas. HERON, Volume 31, No. 4, 1-113.

[28] ALA (2005) American Lifelines Alliance Guidelines for the Design of Buried Steel Pipes.

[29] Honegger DG and Nyman DJ (2004) Guidelines for the seismic design and assessment of natural gas and liquid hydrocarbon pipelines, Prepared for the Pipeline Design, Construction & Operations Technical Committee of Pipeline Research Council International, Inc., Catalog No. L51927.